Supplementary Materials for

Observations and modeling of the elastogravity signals preceding direct seismic waves

Martin Vallée,* Jean Paul Ampuero, Kévin Juhel, Pascal Bernard, Jean-Paul Montagner, Matteo Barsuglia

*Corresponding author. Email: vallee@ipgp.fr

Published 1 December 2017, *Science* **358**, 1164 (2017)
DOI: 10.1126/science.aao0746

This PDF file includes:

Other Supplementary Material for this manuscript includes the following:
(available at www.sciencemag.org/cgi/content/full/358/6367/1164/DC1)

Materials and Methods

Modeling of the prompt elasto–gravity signals

At point $\mathbf{r}$, the elastic displacement $\mathbf{u}$ generated by an earthquake located at $\mathbf{r_s}$ and with normalized moment tensor M_{ij} can be written as (e.g. *32*):

$$u_i(\mathbf{r}, t) = M_{jk} m(t) * \mathcal{G}_{ij,k}(\mathbf{r}, \mathbf{r_s}; t) \tag{S1}$$

where $\mathcal{G}_{ij}$ is the Green's function and m is the temporal moment function of the earthquake (its integral is the earthquake seismic moment). In a realistic medium, $\mathcal{G}_{ij}$ has to be calculated numerically, which is done here using AXITRA (*15*). This code is based on the discrete wavenumber approach (*16*) combined with the reflectivity technique (*33*), and allows to calculate the Green function in a vertically stratified medium. Earth flattening (*33,34*) is introduced to correct for sphericity, as some stations are several thousands of kilometers away from the earthquake. We use here the PREM model (*35*) in the mantle combined with a continental crustal thickness of 40 km.

We use the parameters of the Global Centroid Moment Tensor (*23*) for the source coordinates (latitude=37.52, longitude=143.05, depth=20km), origin time (2011/03/11, 05:46:22.8) and static moment tensor M_{ij} controlled by (strike, dip, rake) = $(203^\circ, 10^\circ, 88^\circ)$. We adopt as moment function m the temporal integral of the isosceles triangular GCMT moment rate function (140 s duration). Its time integral is the GCMT seismic moment ($M_0 = 5.31\,10^{22}$N.m). The centroid formalism only takes into account the first order terms of the effects generated by the spatial and temporal extents of the seismic source (*36*). However, the source of the Tohoku earthquake is compact (250 km x 150 km , e.g. *37*) and the gravity perturbations are long–period (*7*), hence the centroid source description is completely appropriate for most of the stations considered here. We only expect that this simplified formalism can affect the modeling accuracy at

the closest stations (MAJO, INU and SHR), located at distances shorter than 700 km. The latter stations are however mostly included to illustrate why their elasto-gravity signals are smaller than the ones of stations located further away (limited time window compared to earthquake duration and strong cancelling effect of the gravity perturbations by the induced accelerations), and the point-source modeling is sufficient for these purposes.

At time t, the volume V_s^P affected by $\mathbf{u}$ is controlled by the travel–time of the fastest (P) elastic waves :

$$V_s^P(t) = \{\mathbf{r}' \in V \,/\, T^P(\mathbf{r_s}, \mathbf{r}') < t\}, \tag{S2}$$

where V is the volume of the Earth and $T^P(\mathbf{r}, \mathbf{r}')$ is the P–wave travel–time between $\mathbf{r}$ and $\mathbf{r}'$. In an homogeneous medium, V_s^P is an open ball, centered in $\mathbf{r_s}$ and growing with time (Fig. S3); at $t = T_P$, where $T_P = T^P(\mathbf{r_s}, \mathbf{r_0})$ is the P–wave travel–time between the source and the station located in $\mathbf{r_0}$, its radius is the distance between $\mathbf{r_s}$ and $\mathbf{r_0}$. Once $\mathbf{u}$ is calculated using equation (S1) on a grid meshing the volume $V_s^P(T_P)$, the early gravity perturbation $\Delta\mathbf{g}^P$ at times $t < T^P(\mathbf{r_s}, \mathbf{r})$ can be calculated with the relation (*6,7*):

$$\Delta\mathbf{g}^P(\mathbf{r}, t) = G \int_{V_s^P(t)} \frac{\rho(\mathbf{r}')[\mathbf{u}(\mathbf{r}', t) - 3(\mathbf{e_{r'r}}.\mathbf{u}(\mathbf{r}', t))\mathbf{e_{r'r}}]}{|\mathbf{r}' - \mathbf{r}|^3} d\mathbf{r}' \tag{S3}$$

where G is the gravitational constant, ρ is the density, and $\mathbf{e_{r'r}} = (\mathbf{r}' - \mathbf{r})/|\mathbf{r}' - \mathbf{r}|$. Equation (S3) adequately takes into account the density variations in the volume due to compression and dilation, as well as the contributions of the deformation of the Earth's surface and other material interfaces during wave propagation. Observing that $\rho\Delta\mathbf{g}^P$ is instaneously non-zero everywhere in the medium (equation S3), and realizing that this term is itself a distribution of body forces generating elastic waves, there is an evolving volume V_g^P that is a source of elastic waves arriving in $\mathbf{r_0}$ before T_P:

$$V_g^P(t) = \begin{cases} \{\mathbf{r}' \in V \,/\, T^P(\mathbf{r_0}, \mathbf{r}') < T_P - t\} & \text{if } t \geq 0 \\ \varnothing & \text{if } t < 0 \end{cases} \tag{S4}$$

In an homogeneous medium, V_g^P is an open ball centered in $\mathbf{r_0}$, initially with radius equal to the distance between $\mathbf{r_0}$ and $\mathbf{r_s}$, and shrinking with time (Fig. S3). In any medium, there is no intersection between $V_g^P(t)$ and $V_g^P(t)$ for any time t (because $\forall \mathbf{r} \in V, (T^P(\mathbf{r_0}, \mathbf{r}) + T^P(\mathbf{r_s}, \mathbf{r})) \leq T_P$, the only case of equality being when $\mathbf{r}$ is on the P ray between $\mathbf{r_s}$ and $\mathbf{r_0}$). In V_g^P, the gravity perturbation is therefore the unique acting force and the associated waves arriving in $\mathbf{r_0}$ before T_P travel in an otherwise unperturbed medium. We can then use again the Green function representation, with the gravity perturbations acting as force source terms. Taking into account the contribution of all gravity perturbations, the acceleration in $\mathbf{r_0}$ at $t < T_P$ is :

$$\ddot{u}_z^P(\mathbf{r_0}, t) = \frac{d^2}{dt^2} \int_0^{T_P} \int_{V_g^P(\tau)} \rho(\mathbf{r}') \Delta g_i^P(\mathbf{r}', \tau) \mathcal{G}_{iz}(\mathbf{r_0}, \mathbf{r}'; t - \tau) d\mathbf{r}' d\tau \tag{S5}$$

Considering that $\mathcal{G}_{iz}(\mathbf{r_0}, \mathbf{r}'; t-\tau) = 0$ if $(t-\tau) < T^P(\mathbf{r_0}, \mathbf{r}')$ (before the arrival of the P waves), Equation (S5) can be written:

$$\ddot{u}_z^P(\mathbf{r_0}, t) = \frac{d^2}{dt^2} \int_0^{T_P} \int_{V_g^P(t - T^P(\mathbf{r_0}, \mathbf{r}'))} \rho(\mathbf{r}') \Delta g_i^P(\mathbf{r}', \tau) \mathcal{G}_{iz}(\mathbf{r_0}, \mathbf{r}'; t - \tau) d\mathbf{r}' d\tau \tag{S6}$$

or in convolutive form :

$$\ddot{u}_z^P(\mathbf{r_0}, t) = \frac{d^2}{dt^2} \int_{V_0^P(t)} \rho(\mathbf{r}') \Delta g_i^P(\mathbf{r}', t) * \mathcal{G}_{iz}(\mathbf{r}', \mathbf{r_0}, t) d\mathbf{r}' \tag{S7}$$

where

$$V_0^P(t) = V_g^P(t - T^P(\mathbf{r_0}, \mathbf{r}')) = \begin{cases} \{\mathbf{r}' \in V \ / \ T^P(\mathbf{r_0}, \mathbf{r}') < t\} & \text{if } t \leq T_P \\ \varnothing & \text{if } t > T_P \end{cases} \tag{S8}$$

$V_0^P(t)$ has the physical interpretation to be the location of the gravity perturbations that generate elastic waves in $\mathbf{r_0}$ at a given time t ($< T_P$). In an homogeneous medium, V_0^P is an open ball, centered in $\mathbf{r_0}$ and growing with time (Fig. S3); at $t = T_P$, its radius is the distance between $\mathbf{r_s}$ and $\mathbf{r_0}$. In order to practically compute $\ddot{u}_z^P$ with equation (S7), $\Delta \mathbf{g}^P$ and $\mathcal{G}_{iz}$ are calculated on a grid meshing $V_0^P(T_P)$, using equation (S3) and again the AXITRA code, respectively.

Combining equations (S3) and (S7) provides access to the prompt elasto–gravity signal recorded in $\mathbf{r_0}$:

$$\forall t < T_P,\ a_z^P(\mathbf{r_0}, t) = \Delta g_z^P(\mathbf{r_0}, t) - \ddot{u}_z^P(\mathbf{r_0}, t) \tag{S9}$$

The theoretical cancellation between Δg_z^P and $\ddot{u}_z^P$ in an homogeneous medium (see the demonstration in the last subsection of the *Material and Methods*) provides a way to validate the suitability of this approach in a specific case, both from the theoretical and numerical points of view. As shown in Fig. S4, this cancellation is well reproduced when deepening the source and the receiver and considering an homogeneous Earth model instead of the PREM model. This strongly supports the modeling of the elasto–gravity signals provided in this study.

Evaluation of the contribution of additional terms

Other terms contributing to a_z^P :

In equation (S9), we neglect the additional effect on the seismometer of the gravity perturbations related to the Earth displacement u_z^P at the station. This additional term can be written Ku_z^P, where the K factor represents the free–air gravity effect ($2g/R$, where g is gravity at the surface and R the Earth radius) minus the Bouguer anomaly ($2\pi\rho G$). Evaluation of these terms at the surface gives $K \simeq 2.10^{-6} s^{-2}$. When compared to $\ddot{u}_z^P$, this term would be of comparable (or larger) amplitude only for very low frequencies, and has a quadratic decay with increasing frequencies. Practically, even at the lowest frequency considered here (0.002Hz), its relative amplitude is $K/(4\pi^2 0.002^2) \simeq 0.012$. The associated perturbations are at least two orders of magnitude lower than the contributions of Δg_z^P and $\ddot{u}_z^P$ considered in equation (S9).

Validity of the non-gravitational approximation of the wave equation

Seismological problems involving the elastic and gravitational fields can be exactly formulated by a self–gravitating set of equations where both fields are coupled (e.g. equation 4.3 in *6*, coupled with the Poisson equation). This takes in particular into account that seismic waves induce gravity perturbations, which in turn modify the seismic wavefield. These effects are not considered in equations (S1) and (S5-S7), where the Green's functions are computed with the AXITRA method in a non-gravitating medium (considering therefore the classical elasto–dynamic wave equation). However, the relative amplitude of the gravitational effects in the wave equation at a given frequency f depends on the factor $(f_0/f)^2$ where $f_0 = \sqrt{\rho G/\pi}$ (see page 142 in *6*). In the crust and upper mantle, $\rho = 3000 - 5000\ kg/m^3$, which means that even at the lowest frequencies considered here (0.002 Hz), the gravitational effects are on the order of 2%. Thus on the one hand, we can consider that inside V_s^P, $\mathbf{u}$ is accurately computed using the classical elasto–dynamic equation with a force term representing the earthquake source, which leads to equation (S1). And on the other hand, inside V_g^P, we can consider that $\ddot{u}_z^P$ is accurately computed using the classical elasto–dynamic equation with $\rho\Delta\mathbf{g}^P$ as a body–force term (equations S5-S7). The complete resolution of the wave equations in a self-gravitating Earth, which is usually done by a normal–mode approach (e.g. *6*), is therefore not required in this study. The present approach has the practical advantage to compute the prompt elasto–gravity signals without modelling the full wavefield at the station. Normal–mode summation methods would instead require a very high accuracy in order to reproduce these tiny signals without being affected by the much larger amplitude elastic waves (10^5 to 10^6 times larger, see Fig. S1)

Full cancellation of $\Delta\mathbf{g}^P$ by $\ddot{\mathbf{u}}^P$ in an infinite medium

We start from the study of Harms *et al.* (*7*), who derived the gravity perturbation $\Delta\mathbf{g}$ induced by the seismic wavefield $\mathbf{u}$ generated by an earthquake source $\mathbf{f}$ in an infinite elastic space of density ρ_0. Ignoring self–gravitational coupling, the governing equations for that problem are:

$$\rho_0 \ddot{\mathbf{u}} = \nabla \cdot \sigma + \mathbf{f} \tag{S10}$$

$$\nabla^2 \psi = -4\pi\rho_0 G \, \nabla \cdot \mathbf{u} \tag{S11}$$

$$\Delta\mathbf{g} = -\nabla\psi \tag{S12}$$

where σ is the stress tensor and ψ the gravitational potential. The solution features transient gravity changes before the arrival of P waves, which Harms *et al.* (*7*) coined "prompt gravity perturbations". This prompt gravity perturbation is the restriction of the $\Delta\mathbf{g}$ gravity perturbation to times shorter than the hypocentral P–wave arrival time at a given location, and is noted $\Delta\mathbf{g}^P$ as in the main text. Here we show that, in an infinite medium, before the arrival of "direct P waves" from the earthquake source contained in the direct wave field $\mathbf{u}$, the ground acceleration $\ddot{\mathbf{u}}^P$ induced by $\Delta\mathbf{g}^P$ is exactly equal to $\Delta\mathbf{g}^P$.

The momentum equation governing the gravity–induced wavefield $\mathbf{u}^P$, involving the stress tensor σ^P, is

$$\rho_0 \ddot{\mathbf{u}}^P = \nabla \cdot \sigma^P + \rho_0 \, \Delta\mathbf{g}^P \tag{S13}$$

Because $\mathbf{u} = 0$ before direct P waves arrive, we have ignored the term related to advection through the pre–existing gravity gradient $\rho_0 \mathbf{u} \cdot \nabla \mathbf{g_0}$ (where $\mathbf{g_0}$ is the initial gravity, see equation 4.3 in *6*). In a self–gravitating Earth, the equations above should be solved simultaneously. Because here we focus on frequencies significantly higher than $f_0 = \sqrt{\rho_0 G/\pi}$, we can neglect the complete self–gravitational coupling and treat these equations sequentially, similarly as what has been done in the first subsection of the *Material and Methods*.

We use the conventional decomposition of the earthquake source and the direct wave field into P and S terms derived from potentials:

$$\mathbf{f} = \nabla\Phi + \nabla \wedge \mathbf{\Psi} \tag{S14}$$

$$\mathbf{u} = \nabla\phi_s + \nabla \wedge \psi_s \tag{S15}$$

In this formalism, P and S waves are decoupled, and a source term with a scalar potential Φ generates a pure P wave displacement with scalar potential ϕ_s. On the one hand, taking the gradient of equation (9) in Harms *et al.* (*7*), which is valid at all times, we get

$$\nabla\psi = -4\pi\rho_0 G\,\nabla\phi_s \tag{S16}$$

As this equation is a fortiori true before the arrival of the P waves, we have:

$$\Delta\mathbf{g}^P = 4\pi\rho_0 G\,\nabla\phi_s \tag{S17}$$

On the other hand, taking the gradient of equation (16) in Harms *et al.* (*7*), valid before direct P waves arrive, we get

$$\nabla\ddot{\psi} = -4\pi G\nabla\Phi \tag{S18}$$

Writing equation (S18) as

$$-\rho_0\nabla\ddot{\psi} = 4\pi\rho_0 G\,\nabla\Phi\,, \tag{S19}$$

we recognize in the left hand side the second time derivative of the source term $\rho_0\,\Delta\mathbf{g}^P$ ($= -\rho_0\nabla\psi$) that induces $\mathbf{u}^P$ in equation (S13). Because the governing equations are linear, we infer that the wave field displacement $\mathbf{u}^P$ induced by $-\rho_0\nabla\psi$ is related to the wave field displacement $\nabla\phi_s$ induced by $\nabla\Phi$ with

$$\ddot{\mathbf{u}}^P = 4\pi\rho_0 G\,\nabla\phi_s \tag{S20}$$

Comparing equations (S17) and (S20), we conclude that

$$\Delta\mathbf{g}^P = \ddot{\mathbf{u}}^P \tag{S21}$$

This result shows that, in an infinite medium, an accelerometer or gravimeter coupled to the elastic medium, is insensitive to the prompt gravity perturbation $\Delta\mathbf{g}^P$ because of exact cancellation by the gravity–induced ground acceleration $\ddot{\mathbf{u}}^P$. Numerical simulations mimicking the full-space configuration (Fig. S4) well reproduce this theoretical finding.

However, this exact cancellation is not expected to hold in a half–space, owing to free surface effects. After the direct seismic waves reach the free surface, equation (S16) is no longer valid, but requires an additional term that involves the surface deformation (*8*). One particular situation is tractable and provides some insight. Before direct P waves from a buried source arrive at the free surface, $\Delta\mathbf{g}^P$ is the same as in an infinite space and the derivation of $\ddot{\mathbf{u}}^P$ is still valid if in equation (S20) we replace $\nabla\phi_s$ by the displacement field $\nabla\tilde{\phi}_s$ generated by $\nabla\Phi$ in a half–space in the absence of $\nabla \wedge \mathbf{\Psi}$. Note that $\nabla\tilde{\phi}_s$ is not the same as the $\nabla\phi_s$ that may be obtained as an intermediate step in the derivation of the Green's function for Lamb's problem (e.g. *38*), because the sources are different: $\nabla\Phi$ in our problem and $(\nabla\Phi + \nabla \wedge \mathbf{\Psi})$ in Lamb's problem. This difference is significant because P and S potentials are coupled by the free surface boundary conditions. Note also that the source $\nabla\Phi$ is not localized at a point but distributed over the half space:

$$\Phi(\mathbf{r}, t) = \frac{M_{ij}(t)}{2\pi} \frac{\partial^2 1/r}{\partial x_i \partial x_j} \tag{S22}$$

for a double–couple point–source (a generalization of equation 17 in Harms *et al.* *7*). The resulting $\nabla\tilde{\phi}_s$ is not a pure P wave field, but includes S waves generated at the free surface. These S waves contribute to $\ddot{\mathbf{u}}^P$ but not to $\Delta\mathbf{g}^P$. Clearly, in this situation, $\ddot{\mathbf{u}}^P$ and $\Delta\mathbf{g}^P$ are not equal.

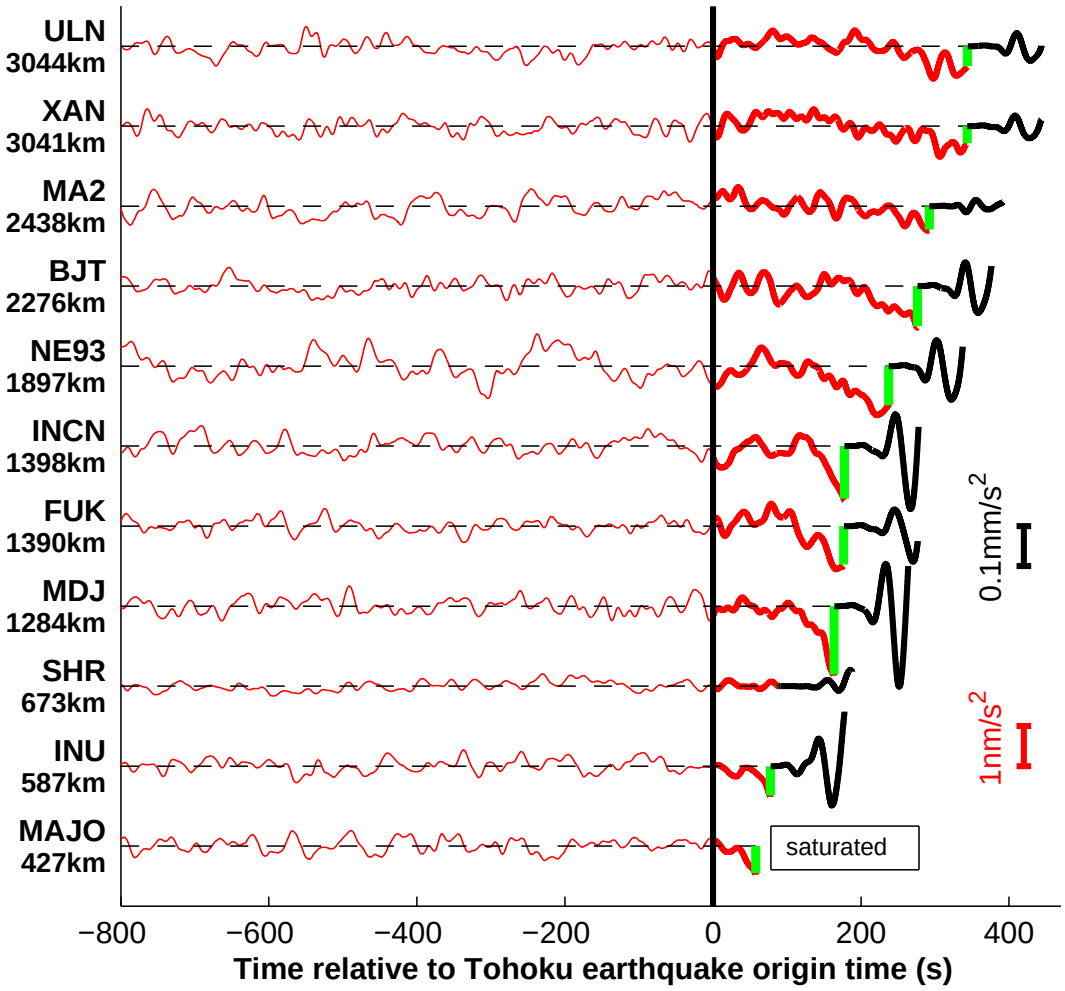

Figure S1: **Acceleration signals in the pre– and and post–P–wave time window**. Signals are filtered in the 0.002–0.03Hz frequency range, in a time window starting 800 s before the earthquake origin time and terminating 100 s after the P–wave arrival (green tick) at each station. Station names and their hypocentral distances in kilometers (following Earth surface) are shown to the left of each signal. Before the P–wave arrival, acceleration signals (a_z^P) and their corresponding scales ($1nm/s^2$) are shown in red (as in Figure 1). After the P–wave arrival, acceleration signals and their corresponding scales ($0.1mm/s^2$) are shown in black. At this 1:100000 scale, post–P– wave signals have similar or larger amplitudes than pre–P–wave signals, meaning that the P–wave elastic signals are typically more 10^5 times larger than a_z^P. This value is even larger if comparing with later elastic arrivals (approaching 10^6), but few stations allow this comparison because of saturation of the signals. This saturation already affects the MAJO station in the 100 s time window following the P–wave arrival.

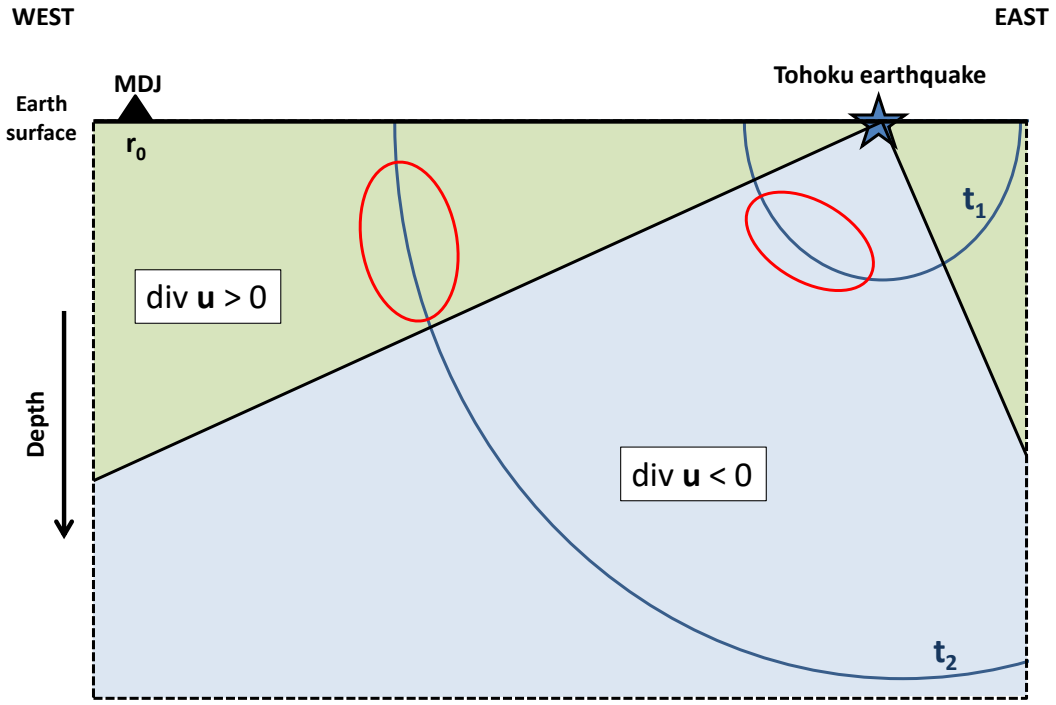

Figure S2: **Illustration of the origins of the Δg_z^P temporal variations, for stations West from the Tohoku earthquake**. We here take the MDJ station (located in $\mathbf{r_0}$) as an example. The blue circles represent two isochrones of the hypocentral P–wave travel–time; the t_1 isochrone illustrates early times after the earthquake origin and t_2 times closer from the P–wave arrival time at MDJ. As a result of the focal mechanism of the Tohoku earthquake, the blue area is compressed by the P waves ($\nabla \cdot \mathbf{u} < 0$) and the green areas are dilated by the P waves ($\nabla \cdot \mathbf{u} > 0$). For a station located at the Earth surface, there are no contributions from Earth surface effects to Δg_z^P and we have $\Delta g_z^P = -G \int_V \rho \nabla \cdot \mathbf{u} \ (\mathbf{e_{rr_0}}.\mathbf{e}_z)/r^2 \, d\mathbf{r}$, where $\mathbf{e}_z$ is the unit vertical vector. From the latter equation, we can figure out which parts of the volume have a dominant effect on Δg_z^P at a given time t: the closest regions from the station where $\nabla \cdot \mathbf{u} \neq 0$ and $\mathbf{e_{rr_0}}.\mathbf{e}_z \neq 0$ are expected to be the main contributors to Δg_z^P. For $t = t_1$ and $t = t_2$, these regions are indicated by the red ellipses. As the sign of $\nabla \cdot \mathbf{u}$ changes for these two ellipses, we expect Δg_z^P to be positive at early times and to become later negative, as numerically simulated in Fig. 2.

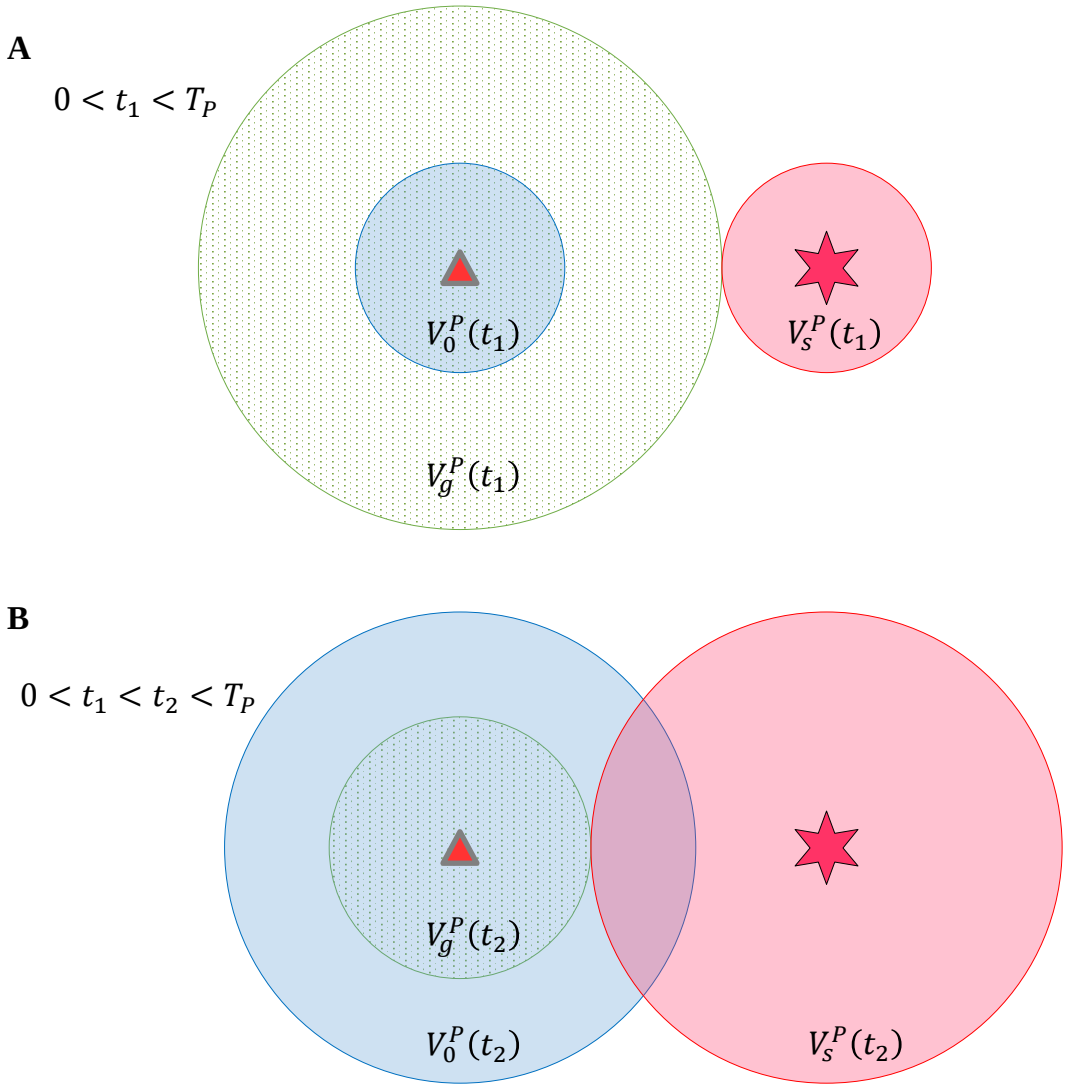

Figure S3: **Illustration of the volumes contributing to the prompt elasto–gravity signals in an homogeneous medium.** The star and triangle are the earthquake and the receiver, respectively. A and B show the configuration at two increasing times before the P hypocentral arrival–time T_P. V_s^P (shaded with red) is the volume affected by elastic displacements directly induced by the earthquake. V_g^P (filled with green dots) is the volume where gravitational perturbations induced by the displacements in V_s^P generate elastic waves arriving before T_P at the receiver. $V_0^P(t)$ (shaded with blue) is the volume that is at the orgin of the latter elastic waves arriving at t at the receiver. All these volumes are open balls in this homogeneous medium (where there is a full cancellation between Δg_z^P and $\ddot{u}_z^P$). However these volumes remain defined in a realistic Earth medium (such as the PREM model used in our simulations) even if their geometries are deformed and possibly cut by the Earth surface. Even in heterogeneous media, there is no intersection between V_s^P and V_g^P.

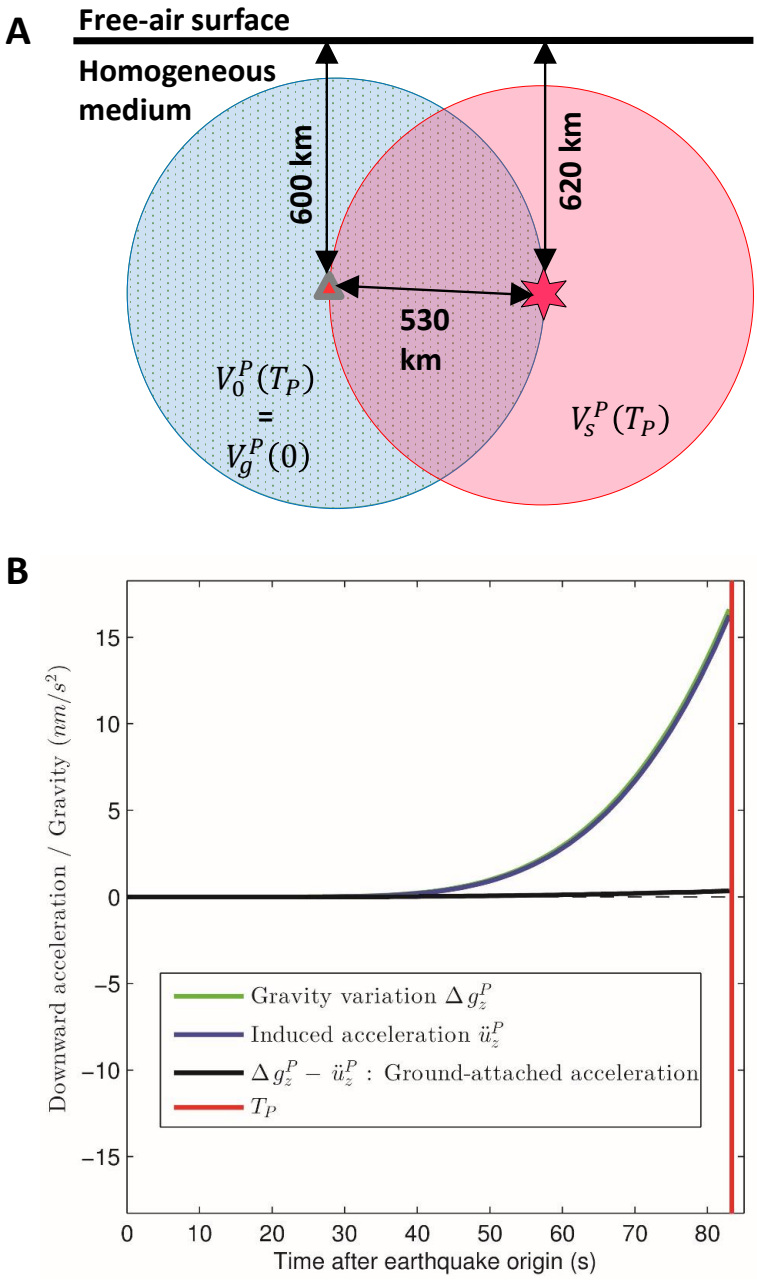

Figure S4: **Validation of the approach in an homogeneous medium.** The configuration shown in A is exactly the one of the INU station, except that (1) the earthquake and station depths have been increased by 600km and (2) the PREM model has been replaced by an homogeneous model ($V_p = 6400m/s$, $V_S = 3700m/s$, $\rho = 2700kg/m^3$). In this case, the 3 volumes V_s^P, V_g^P and V_0^P do not have any interaction with the Earth surface at any time (their maximum extensions are shown), which mimics a fully homogeneous medium. B shows that $\ddot{u}_z^P$ closely follows the evolution of Δg_z^P up to the hypocentral P–wave arrival time, resulting in the expected cancellation of the elasto–gravity signal. All the signals are shown in the [0.002-0.03Hz] frequency range.

Data file S1: (Trait_hplp_and_visu_SAC_for_reproduction.tar): A procedure to reproduce the prompt elasto-gravity signals (shown in Figure 1), starting from the raw broadband signals. By first reading the 'README' file of this directory, the user has :

- Detailed information about the data processing strategy
- A practical way to reproduce numerically the signals (starting from the raw data and metadata included in the directory), using a procedure written for the widely used SAC software.

References

1. S. Okubo, Gravity and potential changes due to shear and tensile faults in a half-space. *J. Geophys. Res.* **97**, 7137–7144 (1992). doi:10.1029/92JB00178

2. Y. Imanishi, T. Sato, T. Higashi, W. Sun, S. Okubo, A network of superconducting gravimeters detects submicrogal coseismic gravity changes. *Science* **306**, 476–478 (2004). doi:10.1126/science.1101875 Medline

3. K. Matsuo, K. Heki, Coseismic gravity changes of the 2011 Tohoku-Oki earthquake from satellite gravimetry. *Geophys. Res. Lett.* **38**, L00G12 (2011). doi:10.1029/2011GL049018

4. Japan Meteorological Agency, http://www.jma.go.jp/jma/indexe.html

5. Y. Okada, Preliminary report of the 2011 off the Pacific coast of Tohoku Earthquake, http://www.bosai.go.jp/e/pdf/Preliminary_report110328.pdf (2011).

6. F. A. Dahlen, J. Tromp, *Theoretical Global Seismology* (Princeton Univ. Press, Princeton, 1998).

7. J. Harms, J.-P. Ampuero, M. Barsuglia, E. Chassande-Mottin, J.-P. Montagner, S. N. Somala, B. F. Whiting, Transient gravity perturbations induced by earthquake rupture. *Geophys. J. Int.* **201**, 1416–1425 (2015). doi:10.1093/gji/ggv090

8. J. Harms, Transient gravity perturbations from a double-couple in a homogeneous half space. *Geophys. J. Int.* **205**, 1153–1164 (2016). doi:10.1093/gji/ggw076

9. J.-P. Montagner, K. Juhel, M. Barsuglia, J. P. Ampuero, E. Chassande-Mottin, J. Harms, B. Whiting, P. Bernard, E. Clévédé, P. Lognonné, Prompt gravity signal induced by the 2011 Tohoku-Oki earthquake. *Nat. Commun.* **7**, 13349 (2016). doi:10.1038/ncomms13349 Medline

10. Incorporated Research Institutions for Seismology (IRIS), http://ds.iris.edu/ds/nodes/dmc/

11. F-net Broadband Seismograph Network, http://www.fnet.bosai.go.jp

12. Information on materials and methods is available in the supplementary materials.

13. GEOSCOPE Observatory, http://geoscope.ipgp.fr/index.php/en/

14. Waveform Quality Center, Lamont-Doherty Earth Observatory; http://www.ldeo.columbia.edu/ekstrom/Projects/WQC/MONTHLY_HTML/

15. F. Cotton, O. Coutant, Dynamic stress variations due to shear faults in a plane-layered medium. *Geophys. J. Int.* **128**, 676–688 https://www.isterre.fr/annuaire/pages-web-du-personnel/olivier-coutant/article/logiciels-softwares?lang=fr (1997). doi:10.1111/j.1365-246X.1997.tb05328.x

16. M. Bouchon, A simple method to calculate Green's functions for elastic layered media. *Bull. Seismol. Soc. Am.* **71**, 959–971 (1981).

17. T. H. Heaton, Correspondence: Response of a gravimeter to an instantaneous step in gravity. *Nat. Commun.* **8**, 966 (2017). doi:10.1038/s41467-017-01348-z Medline

18. H. Houston, Influence of depth, focal mechanism, and tectonic setting on the shape and duration of earthquake source time functions. *J. Geophys. Res.* **106**, 11137–11150 (2001). doi:10.1029/2000JB900468

19. M. Vallée, Source time function properties indicate a strain drop independent of earthquake depth and magnitude. *Nat. Commun.* **4**, 2606 (2013). doi:10.1038/ncomms3606 Medline

20. L. Ye, T. Lay, H. Kanamori, L. Rivera, Rupture characteristics of major and great ($M_w \geq 7.0$) megathrust earthquakes from 1990 to 2015: 1. Source parameter scaling relationships. *J. Geophys. Res.* **121**, 826–844 (2016). doi:10.1002/2015JB012426

21. M. E. Pasyanos, D. S. Dreger, B. Romanowicz, Towards real-time determination of regional moment tensors. *Bull. Seismol. Soc. Am.* **86**, 1255–1269 (1996).

22. B. Delouis, FMNEAR: Determination of focal mechanism and first estimate of rupture directivity using near-source records and a linear distribution of point sources. *Bull. Seismol. Soc. Am.* **104**, 1479–1500 (2014). doi:10.1785/0120130151

23. G. Ekström, M. Nettles, A. M. Dziewonski, The global CMT project 2004–2010: Centroid-moment tensors for 13,017 earthquakes. *Phys. Earth Planet. Inter.* **200–201**, 1–9 (2012). doi:10.1016/j.pepi.2012.04.002

24. H. Kanamori, L. Rivera, Source inversion of W phase: Speeding up seismic tsunami warning. *Geophys. J. Int.* **175**, 222–238 (2008). doi:10.1111/j.1365-246X.2008.03887.x

25. M. Vallée, J. Charléty, A. M. G. Ferreira, B. Delouis, J. Vergoz, SCARDEC: A new technique for the rapid determination of seismic moment magnitude, focal mechanism and source time functions for large earthquakes using body wave deconvolution. *Geophys. J. Int.* **184**, 338–358 (2011). doi:10.1111/j.1365-246X.2010.04836.x

26. M. Ando, K. Ishidoshiro, K. Yamamoto, K. Yagi, W. Kokuyama, K. Tsubono, A. Takamori, Torsion-bar antenna for low-frequency gravitational-wave observations. *Phys. Rev. Lett.* **105**, 161101 (2010). doi:10.1103/PhysRevLett.105.161101 Medline

27. D. J. McManus, P. W. F. Forsyth, M. J. Yap, R. L. Ward, D. A. Shaddock, D. E. McClelland, B. J. J. Slagmolen, Mechanical characterisation of the TorPeDO: A low frequency gravitational force sensor. *Class. Quantum Gravity* **34**, 135002 (2017). doi:10.1088/1361-6382/aa7103

28. A.-M. V. Moody, H. J. Paik, E. R. Canavan, Three-axis superconducting gravity gradiometer for sensitive gravity experiments. *Rev. Sci. Instrum.* **73**, 3957–3974 (2002). doi:10.1063/1.1511798

29. J. H. Paik, C. E. Griggs, M. V. Moody, K. Venkateswara, H. M. Lee, A. B Nielsen, E. Majorana, J. Harms, Low-frequency terrestrial tensor gravitational-wave detector. *Class. Quantum Gravity* **33**, 075003 (2016). doi:10.1088/0264-9381/33/7/075003

30. M. Hohensee, S.-Y. Lan, R. Houtz, C. Chan, B. Estey, G. Kim, P.-C. Kuan, H. Müller, Sources and technology for an atomic gravitational wave interferometric sensor. *Gen. Relativ. Gravit.* **43**, 1905–1930 (2011). doi:10.1007/s10714-010-1118-x

31. R. Geiger, Future gravitational wave detectors based on atom interferometry, in *An Overview of Gravitational Waves: Theory and Detection*, G. Auger, E. Plagnol, Eds. (World Scientific, 2017).

32. K. Aki, P. G. Richards, *Quantitative Seismology* (University Science Books, ed. 2, Sausalito, 2002).

33. G. Müller, The reflectivity method: A tutorial. *J. Geophys.* **58**, 153–174 (1985).

34. G. Müller, Earth-flattening approximation for body waves derived from geometric ray theory improvements, corrections and range of applicability. *J. Geophys.* **42**, 429–436 (1977).

35. A. M. Dziewonski, D. L. Anderson, Preliminary reference Earth model. *Phys. Earth Planet. Inter.* **25**, 297–356 (1981). doi:10.1016/0031-9201(81)90046-7

36. A. M. Dziewonski, T. A. Chou, J. H. Woodhouse, Determination of earthquake source parameters from waveform data for studies of global and regional seismicity. *J. Geophys. Res.* **86**, 2825–2852 (1981). doi:10.1029/JB086iB04p02825

37. Q. Bletery, A. Sladen, B. Delouis, M. Vallée, J.-M. Nocquet, L. Rolland, J. Jiang, A detailed source model for the M_w 9.0 Tohoku-Oki earthquake reconciling geodesy, seismology and tsunami records. *J. Geophys. Res.* **119**, 7636–7653 (2014). doi:10.1002/2014JB011261

38. L. R. Johnson, Green's function for Lamb's problem. *Geophys. J. Int.* **37**, 99–131 (1974). doi:10.1111/j.1365-246X.1974.tb02446.x